



1 **Monitoring crustal CO₂ flow: methods and their applications to**
2 **the mofettes in West Bohemia**
3

4 Tomáš Fischer, Josef Vlček, Martin Lanzendörfer
5 Charles University, Faculty of Science, Prague, Czechia
6

7
8 **Abstract** Monitoring of CO₂ degassing in seismoactive areas allows the study of correlations of gas release and
9 seismic activity. Reliable continuous monitoring of the gas flow rate in rough field conditions requires robust methods
10 capable of measuring gas flow at different types of gas outlets such as wet mofettes, mineral springs and boreholes.
11 In this paper we focus on the methods and results of the long-term monitoring of CO₂ degassing in the West
12 Bohemia/Vogtland region in Central Europe, which is typified by the occurrence of earthquake swarms and
13 emanations of carbon dioxide of magmatic origin. Besides direct flow measurement using flowmeters, we introduce
14 a novel indirect technique based on quantifying the gas bubble contents in a water column, which is capable of
15 functioning in severe environmental conditions. The method calculates the mean bubble fraction in a water-gas
16 mixture from the pressure difference along a fixed depth interval in a water column. Laboratory tests indicate the
17 nonlinear dependence of the bubble fraction on the flow rate, which is confirmed by empirical models found in the
18 chemical and nuclear engineering literature. Application of the method in a pilot borehole shows a high correlation
19 between the bubble fraction and measured gas flow rate. This was specifically the case of two coseismic anomalies
20 in 2008 and 2014, when the flow rate rose during a seismic swarm to a multitude of the pre-seismic level for several
21 months and was followed by a long-term flow rate decline. However, three more seismic swarms occurring in the
22 same fault zone were not associated with any significant CO₂ flow anomaly. We surmise that this could be related to
23 the slightly farther distance of the hypocenters of these swarms than the two ones which caused the coseismic CO₂
24 flow rise. Further long-term CO₂-flow monitoring is required to verify the mutual influence of CO₂ degassing and
25 seismic activity in the area.

26
27
28



29 1. Introduction

30 Long-term monitoring of crustal fluids activity provides a unique opportunity to better understand the relationships
31 among tectonic processes, seismic activity and migration of fluids in the Earth crust. Carbon-dioxide of deep origin
32 represents a link between deep seated magmatic sources of CO₂, the fluid migration paths in the crust, which are
33 controlled by the tectonic stress field, and the earth surface. The presented study is focused to monitoring of CO₂
34 degassing in the West Bohemia/Vogltand area, which is located in the western part of the Bohemian Massif (BM), the
35 largest coherent surface exposure of basement rocks in central Europe. The western BM is hosting a junction of three
36 tectonometamorphic units, Saxothuringian, Teplá-Barrandian and Moldanubian (Franke, 2000). It is intersected by
37 two regional tectonic structures, the NE-SW trending Eger Rift (ER) and NNW-SSE trending Mariánské Lázně Fault
38 (MLF) (Fig. 1).

39 The Tertiary ER is a 300 km long striking structure characterized by elevated heat flow and Cenozoic volcanism and
40 its formation is thought to be related to Alpine collision (Ziegler, 1992). The Late-Variscan MLF was reactivated
41 several times during the geological history up to Cenozoic when it participated in the formation of the Cheb Basin
42 (CB). CB is typified by a blocky structural fabric due to a network of faults. Besides the NNW and NW
43 morphologically expressed marginal faults also faults striking NE, E-W and N-S were identified within the basin
44 (Špičáková et al., 2000; Bankwitz et al., 2003).

45 The present geodynamic activity is manifested by earthquake swarms, massive CO₂ degassing of mantle origin and
46 Quaternary volcanism (Fischer et al., 2014). Seismic activity in the form of earthquake swarms is concentrated in the
47 area of CB, in particular the Nový Kostel focal zone (Fig. 1), where more than 80% of seismic energy is released in
48 frames of the whole seismogenic region. Here the hypocenters form a N-S trending, steeply dipping belt in the depth
49 range from 6 to 10 km; however, no clear fault outcrop has been identified that would match the focal zone geometry.
50 The prevailing focal mechanisms coincide very well with the orientation of the fault zone of 169°. Inversion of focal
51 mechanisms for stress field yields maximum compression direction in the range N135–155°E, which coincides well
52 with the average direction N144°E in Western Europe (Fischer et al., 2014). This direction is however parallel to the
53 strike of the MLF, which indicates a passive role of the MLF in the present stress field (Vavryčuk, 2011).

54 The strongest earthquakes usually do not exceed M_L 4.5, as was the case of all the eight major instrumentally recorded
55 swarms between 1985 and 2018.

56 The concentration of the geodynamic phenomena in this small region is not clearly understood. Some authors relate
57 this seismic activity to intersecting crustal faults (e.g., Bankwitz et al., 2003) or to fluids of mantle origin (e.g., Bräuer
58 et al., 2003; Babuška et al., 2016), which could originate from active magmatic underplating (Hrubcová et al., 2017).
59 The degassing occurs in the form of CO₂-rich mineral waters and wet and dry mofettes in several degassing fields.
60 Carbon dioxide is the carrier phase for mantle-derived minor components such as helium, the isotope ratios of which
61 are the best tool to determine whether the fluids are of crustal or mantle-derived origin; high ³He/⁴He ratios indicate
62 that ascending gases are of mantle origin (Bräuer et al., 2003).

63 Gas flow is concentrated in three degassing centers: Cheb Basin, Mariánské Lázně, and Karlovy Vary (KV) (Weinlich
64 et al., 1999; Geissler et al., 2005; Kämpf et al., 2007). They are characterized by a high gas flow with CO₂
65 concentrations of more than 99 vol. %. Cheb Basin also has the highest concentration of seismic activity, which makes



66 it ideal for studying the relations between seismicity and gas flow. Interestingly, numerous studies of the local
67 earthquake swarms show that they may be related to pressurized fluid in the crust and the ascent of gas. This has been
68 pointed out by numerous researchers including Špičák and Horálek (2000), Hainzl and Fischer (2002), Fischer and
69 Horálek (2005) and Hainzl et al. (2016), based on space-time analysis of the seismicity, Horálek et al. (2002),
70 Vavryčuk (2002) and Vavryčuk and Hrubcová (2017), on the basis of moment tensor analysis, and Dahm and Fischer
71 (2014), and Bachura and Fischer (2016), based on Vp/Vs analysis of the volume of hypocenters. The last two studies
72 show that compressible fluids are required to explain the low velocity ratio observed in the course of seismic activity.
73 The gases produced in the West Bohemia/Vogtland mineral springs and mofettes show high $^3\text{He}/^4\text{He}$ ratios; these are
74 significantly higher than the average continental crust, indicating their mantle-derived origin. Also, the $\delta^{13}\text{C}$ values in
75 the CO_2 -rich gas escapes indicate their origin in the upper mantle (Weinlich *et al.*, 1999; Bräuer *et al.*, 2003). The
76 highest portions of mantle-derived helium (up to 6 R_a , where R_a corresponds to the $^3\text{He}/^4\text{He}$ ratio of the atmosphere)
77 were found in the CB; the KV degassing center has the lowest $^3\text{He}/^4\text{He}$ ratios of 2.5 R_a . Lower He-isotope ratios (e.g.
78 $^3\text{He}/^4\text{He} < 6R_a$) probably reflect the gas mixing with crustal-derived He along fluid pathways (Bräuer *et al.*, 2008).
79 CO_2 flow monitoring in West Bohemia has been conducted since the 1990s in a rather discontinuous way. The longest-
80 running observation project is probably the monitoring of Radon activity in Bad Brambach (Heinicke and Koch, 2000;
81 Koch et al., 2003), which has been conducted since 1989.
82 Another long-time monitoring was carried out as part of the “Research of CO_2 pressure field in the area of West
83 Bohemian spas” project funded by the Ministry of the Environment of the Czech Republic from 1996 to 2005. Gas
84 flow in open boreholes and gas pressure in closed boreholes was monitored at 11 gas escape sites in the Cheb Basin
85 and near Mariánské Lázně (Škuthan et al., 2001, Hron et al., 2006). Monitoring of pressure in a closed well was
86 preferred at many project sites since the functioning of mechanical flowmeters was unreliable due to condensation
87 and freezing. A different type of CO_2 flow monitoring was carried out by Faber et al. (2009), who measured diffuse
88 gas flow by determining CO_2 concentration in soil gas at two stations in the Nový Kostel fault zone. CO_2 flow
89 monitoring was also conducted by Heinicke (personal communication) in the Bublák mofette from 2008 to 2014 by
90 recording the acoustic noise of bubbles below the water table, a method which is similar to that used by Koch et al.
91 (2003). No convincing observation of seismogenic CO_2 flow anomaly was, however, presented in the above-
92 mentioned studies.
93 Mapping of CO_2 emanations was conducted in the area by Nickschick et al. (2015). They used an infrared gas analyzer
94 and accumulation chambers to measure CO_2 flux and CO_2 soil concentration in the mofette field of Hartoušov and
95 found that the diffuse gas flow in dry vents accounts for a high portion of the mofette field’s total gas production.
96 The measurement of CO_2 flow presented in this paper began in 2009 in the Hartoušov mofette field with the use of a
97 laboratory chamber flowmeter. Despite problems from the condensation of moisture and freezing temperatures, which
98 resulted in time series gaps, we observed a massive post-seismic CO_2 flow increase shortly after the first M_L 3.5
99 mainshock of the 2014 seismic sequence. A comparison with the fault valve model showed a striking fit, which
100 indicated that the earthquake fracture released gas accumulated in the reservoir beneath hypocenters (Fischer et al.,
101 2017). This gave us a reason to extend the monitoring and test different, more durable, gas flow measurement methods.
102 In this paper, we introduce the principles for our approaches and give a basic comparison of them. We also present



103 the data recorded from the Hartoušov, Bublák, Soos and Prameny stations and evaluate their response to air pressure
104 and temperature and their possible relation to seismicity.

105

106 2. Data and methods

107 Two types of CO₂ degassing are observed in West Bohemia/Vogtland: (i) diffuse gas flow in soil and (ii) massive gas
108 production in mofettes and mineral springs. While gas diffusion in soil is influenced by soil moisture and other local
109 conditions, among other factors, gas flow in massive sources is independent of environmental conditions and should
110 reflect the influence of the gas source at in the depth. The deep roots of CO₂ mofettes were also documented by a
111 massive increase in CO₂ flow in the Hartoušov mofette that began about four days after the start of seismic activity in
112 2008 and 2014 (Fischer et al., 2017). This points to the relatively fast speed of gas migration in the upper crust and
113 qualifies mofettes as favorable places to monitor the amount of leaking gas. Since 2015, the current monitoring at
114 Hartoušov has been extended to other places in order to provide robust measurements capable of recording possible
115 future gas anomalies at multiple sites. Because the conditions differed among the monitored sites, different
116 measurement methods were designed. In this study, we distinguish between *direct* and *indirect* gas flow measurement
117 methods (Camarda et al. 2006). The direct methods directly record the volume of gas per minute and require that gas
118 flow be captured by a funnel or borehole. The indirect methods either involve deriving gas flow from the bubble
119 fraction in water (pressure probes are placed beneath the water table), or rely on measuring gas overpressure in a
120 closed borehole or, finally, they calculate CO₂ flux from the concentration of gradients in the soil (Baubron et al.,
121 1990). The dynamic concentration method is based on measuring the CO₂ content in a mixture of soil gas and air
122 obtained by a special probe placed vertically in the soil. The dynamic concentration is proportional to the soil CO₂
123 flux according to an empirical relationship, which depends on soil permeability (Gurrieri and Valenza, 1988).

124

125 *Figure 1.*

126 2.1 Monitoring network

127 Five gas escape sites were monitored in the period described: *Hartoušov*, *Bublák*, *Soos*, *Dolní Částkov* and *Prameny*
128 (see the map in Fig. 1 and photos in Fig. 2). While the first three are located in mofette fields, the remaining are
129 boreholes which tap mineral spring sources.

130 The pilot site of *Hartoušov* is located in a wooden hut above a 28.2 m deep borehole, which taps a CO₂ saturated,
131 pressurized aquifer. The plastic borehole casing, with an inner diameter of 115 mm, is perforated in the depth range
132 of 20-28 m. Water level measurements date back to 2007, and gas flow has been measured here using a drum chamber
133 gas flowmeter since 2009. The sensitivity of this type of instrument to environmental conditions (freezing or
134 evaporation of the working liquid) caused gaps in the recorded time series. Since 2013, there have only been brief
135 gaps thanks to the use of a different type of working liquid, improvements in the condenser separation and thermal
136 insulation. This direct field gas flow measurement is used as a reference for testing different flow measurement devices



137 prior to their installation at other sites. Additional permanent measurements include water pressure in several depth
 138 levels, water temperature and air temperature and pressure.
 139 The *Bublák* station has been located in a natural mofette in a swamp since 2015. To avoid interfering with natural
 140 conditions at this site, the equipment is buried underground, which does not allow for direct gas flow measurement.
 141 Instead, the differential water level is measured and used as a proxy for the volumetric fraction of free gas in water,
 142 see section 2.3. Because of the rising bubbles, the water does not freeze in winter, making this measurement quite
 143 stable. The *Soos* station has been located in a natural mofette field since 2015, and the gas from a single mofette is
 144 captured by a funnel allowing for direct gas flow measurement. The small size of the metal box shelter and the need
 145 to use battery power, however, do not make it possible to prevent the freezing of the system in winter. The water level
 146 and temperature in the mofette and the volumetric fraction of free gas are measured here using an electric resistivity
 147 probe. In *Dolní Částkov*, the gas escapes both through a shallow borehole and the surrounding soil, which makes the
 148 flow measurements rather unstable. The *Prameny* station is located on top of a 100 m deep closed borehole (HJ-3A,
 149 drilled 1994) with degassing mineral water. Conditions at this site allow only for the measurement of the water level,
 150 temperature and wellhead gas pressure, which have been available since 2009.

151

152 *Figure 2*.

153 Table 1. CarbonNet monitoring network.

Station name and code	Environment	Methods
<i>Bublák</i> <i>BUB</i>	<i>Natural mofette</i>	<i>Water temperature, two pressure heads (sensor depths 0.7 and 1.4 m)</i>
<i>Hartoušov</i> <i>HAR</i>	<i>30m deep open borehole VP8303</i>	<i>Air temperature, barometric pressure, three pressure heads (sensor depths 4.45, 5.45 and 27.2 m), water temperature, gas flow rate, differential pressure in the well</i>
	<i>105.8m deep closed borehole</i>	<i>Pressure head (sensor depth 92m), water temperature, absolute wellhead pressure</i>
<i>Prameny</i> <i>PRA</i>	<i>100m deep open borehole HJ-3A</i>	<i>Pressure head (sensor depth 4.5 m), water temperature, absolute wellhead pressure</i>
<i>Soos</i> <i>SOO</i>	<i>Natural mofette</i>	<i>Pressure head (sensor depth 1.5 m), water temperature, water resistivity</i>
<i>Dolní Částkov</i> <i>DCA</i>	<i>10 m deep open borehole</i>	<i>Gas flow rate</i>



154

155 **2.2 Direct CO₂ flow measurement methods**

156 Long-term gas flow monitoring in the field must meet various requirements. It should provide sufficiently accurate
157 data of gas flow, which may contain dirt particles and moisture in changing field conditions of temperature, humidity
158 and air pressure. The presence of carbon dioxide further creates a highly corrosive environment, which the sensors
159 should withstand. Commercial flowmeters are usually not designed to meet these demands. We have tested (at SOOS
160 and Dolní Částkov stations) the *MEMS* (Micro-Electro-Mechanical Systems) *flowmeter*, which is based on heat
161 convection in moving gas. It works on the principle of a wheatstone bridge, where changes in the resistivity of the
162 resistor are measured according to the temperature changes caused by the flow of gas through a heater placed in the
163 middle of the sensor (Dmytriw et al., 2007). These low-cost sensors, however, failed in our tests. None of the MEMS
164 flowmeters tested measured for longer than 4 months, despite the installation of filters to capture solid particles and
165 moisture from the gas before entering the sensor. A popular way of measuring gas flow is the *Venturi type flowmeter*,
166 which works by measuring the drop-in pressure at a constriction in a tube. Our tests of similar devices failed due to
167 temperature drifts of the sensor and electronics, which were of the same order as the CO₂ flow variations. Direct flow
168 measurement methods also include the *acoustic method* based on the Doppler effect, which is commonly used for
169 water flow measurement. This, however, does not appear to be suitable for gas, which contains fewer particles acting
170 as diffractors than liquid.

171 The standard *flowmeters with rotating mechanical parts* driven directly by the gas flow were also found not suitable
172 due to the corrosive CO₂ environment. Better performance was achieved with a *drum-type chamber flowmeter*, which
173 contains a revolving measuring drum within a packing liquid (we use low-viscosity oil). The measuring drum
174 compulsorily measures volume by periodically filling and emptying four rigid measuring chambers. This *chamber*
175 *laboratory instrument* was found suitable for field measurement, where sufficient space and non-freezing temperatures
176 can be guaranteed. It has been used as the primary flowmeter at the Hartoušov station.

177

178 **2.3 Indirect CO₂ flow measurement methods**

179 **Gas pressure in a closed borehole**

180 In a closed borehole tapping a gas-saturated aquifer an overpressure builds up whose magnitude has been speculated
181 to reflect the amount of gas entering the aquifer from below (e.g. Hron and Škuthan, 2006). However, a profound
182 discussion of how exactly the deep CO₂ leakage affects the measured overpressure is still absent, to the best of our
183 knowledge. Considering a CO₂ flux $q = q_1 + q_2$ summing the flux through the ceiling of the aquifer in the vicinity
184 of the borehole, q_1 and the possible gas leakage through the borehole, q_2 , and assuming simply that the borehole
185 overpressure p is proportional to the both, then p follows the equation

$$186 \quad p = \frac{q}{K_1 + K_2},$$

187 where K_1 and K_2 are the permeability factors related to the ceiling of the aquifer and to the borehole sealing,
188 respectively. Hence the measured overpressure is proportional to the gas flux controlled by deep processes, but also



189 influenced by the permeability of the superficial layer as well as by any possible leaks through the wellhead. In
190 particular, any variation in sealing layer properties, caused e.g. by the actual weather conditions, is then directly
191 projected onto the pressure measured.

192 Accordingly, in spite of the easy implementation of the pressure measurements in a closed borehole, we used this
193 method only at the *Prameny* site, where technical and logistic conditions did not allow the installation and maintenance
194 of a flow measurement. Excessive influence of K_1 on the measured pressure can be suppressed by introducing a
195 controlled leakage in the wellhead, which ensures that K_2 is not small in comparison to K_1 as has been implemented
196 at *Prameny* station.

197

198 **Bubble fraction in water**

199 We have used the bubble fraction monitoring method since observing a striking coincidence between the gas flow rate
200 and groundwater level (see later in this paragraph) increase in the Hartoušov borehole during the 2014 seismic
201 sequence (Fischer et al., 2017). Within a few months after the beginning of the sequence, the gas flow rate in the
202 borehole increased fivefold and the measured water level by more than 1 m. Since then, both quantities have indicated
203 an overall gradual decrease back to their original levels.

204 Instead of the notion of groundwater level, adopted in (Fischer et al., 2017) and other works, we stick to the more
205 strictly defined terms *pressure head* and *hydraulic head* in the present paper, which is due a few explanatory
206 comments. Within a steady water column resting in a borehole (or a narrow mofette), the hydraulic head (defined as
207 the sum of the pressure head and elevation) is independent of the elevation and is referred to as the groundwater level,
208 as it coincides with the elevation of the free water surface observed in the borehole. This is why the exact elevation of
209 the actual placement of the pressure probes in the borehole is usually disregarded, and the term groundwater level is
210 used somewhat loosely without risk of any confusion. In the case of a continuous bubbly flow through the borehole,
211 however, hydraulic head is not a depth-independent quantity, but rather inevitably increases with elevation. An
212 intuitive explanation is that the mean density of the water - gas bubbles mixture is markedly lower than that of water
213 (this is, however, merely an approximation, see also section 2.5). Following this simple concept, the density of the
214 mixture would be (disregarding the density of the gas CO₂ as negligible)

$$215 \quad \rho(z) = (1 - \phi(z))\rho_w, \quad (1)$$

216 where $\phi(z)$ denotes the volumetric fraction of bubbles in the water column profile at elevation z , and ρ_w stands for
217 the mass density of the water in the well (say, clear water at a given constant temperature). Denoting by $\psi(z)$ the
218 pressure head, related to the actual pressure $p(z)$ through $p(z) = \rho_w g \psi(z) + b$ with g being the gravitational
219 acceleration and b the barometric pressure (Fig. 3a), and denoting by $h(z) = \psi(z) + z$ the hydraulic head, we assert
220 that the difference in the measured pressures, pressure head and hydraulic head equals

$$221 \quad p(z_1) - p(z_2) = p_1 - p_2 = \int_{z_1}^{z_2} \rho(z) g \, dz$$
$$222 \quad \Rightarrow \psi_1 - \psi_2 = \int_{z_1}^{z_2} (1 - \phi(z)) \, dz \quad (2)$$
$$223 \quad \Rightarrow h_2 - h_1 = \int_{z_1}^{z_2} \phi(z) \, dz,$$



224 i.e. the hydraulic head $h(z)$ measured in the borehole increases with elevation by a factor equal to the volumetric
225 fraction of the bubbles in the borehole profile. Here, for the sake of brevity, we abstract from the time dependence of
226 all quantities.

227 *Figure 3*

228

229 The mean bubble fraction within the measured section of the water column can thus be defined as

$$230 \quad \overline{\phi}_{12} = \frac{h_2 - h_1}{z_2 - z_1} = 1 - \frac{\psi_1 - \psi_2}{z_2 - z_1} \quad (3)$$

231 As the ascending gas bubbles expand due to the decreasing pressure, both the volumetric flux of the gas and the bubble
232 fraction $\phi(z)$ increase correspondingly with elevation. In order to obtain a quantity independent of the depths of the
233 pressure probes, a further correction needs to be applied. A reasonable approximation can be obtained based on the
234 following simplification. We assume that the gas expands isothermally, so that its volumetric flux is inversely
235 proportional to pressure, and that the bubble fraction is approximately proportional to the volumetric flux, so that we
236 can write

$$237 \quad \phi(z) = \phi_0 \frac{p_0}{p(z)}$$

238 where ϕ_0 represents the bubble fraction at the reference pressure p_0 (which we later set as 100 kPa). Further,
239 approximating the pressure profile between the two pressure probes by a linear function

240

$$241 \quad p(z) = p_1 + \frac{z - z_1}{z_2 - z_1} (p_2 - p_1)$$

242

243 we obtain (by substituting $\phi(z)$ to (2) and integrating) the formula for ϕ_0 , let us call this the projected bubble fraction,

244

$$245 \quad \phi_0 = \overline{\phi}_{12} \frac{p_2 - p_1}{p_0 \ln(p_2/p_1)} \quad (4)$$

246

247 One should note that the quantity obtained here is subject to some uncertainty due to a number of simplifications, and
248 that it only gives the approximated volumetric fraction and not the gas flow rate itself (see section 2.5).

249 In the Hartoušov borehole, the pressure head had been measured until September 2018 by one pressure gauge in the
250 depth of 8 meters, well above the bubble entry point. In (Fischer et al., 2017), the corresponding hydraulic head was
251 referred to as the groundwater level. As proposed in the paper, we split its time variation into two parts: the variation
252 (a) of the hydraulic head $h_e(t)$ at the bottom of the bubble flow column and (b) of its increase through the column due
253 to the gas bubbles. The optimal solution to obtain data for (a), which was implemented in Hartoušov in late 2018, is
254 to measure the pressure head in a depth beneath the bubble entry point directly by a dedicated pressure probe (Fig 3b).
255 While direct measurement was unavailable, it was supposed that (a) is given only by the surrounding hydrogeologic
256 situation and is unaffected by the gas flow. A single measurement of the pressure at the bubble occurrence depth by
257 (Fischer et al., 2017), corrected by a continuous pressure head record from a nearby observation well in Hrčín 8 km
258 apart, which is not affected by the CO₂ gas flow, was used as $h_e(t)$. Note that $h_e(t)$ also describes the hydraulic head
259 in any depth beneath the occurrence of bubbles. While (Fischer et al., 2017) considered the possibility that the gas



260 exsolution depth varies with time, we argue here (see section 2.4) that the gas bubbles have to appear at the penetrated
261 section of the Hartoušov borehole. This allows us to determine the mean volumetric fraction of the bubbles using eq.
262 (3) with $h_1(t) = h_m(t)$ being the hydraulic head measured at the depth $d_m = 4$ m, and $h_2(t) = h_e(t)$ being the hydraulic
263 head measured in any depth below the bubble entry depth, which we suppose to be at the upper part of the penetrated
264 section at $d_e = 20.5$ m (Fig.3).

265 In Fig. 4 the record of $h_e(t)$ and $h_m(t)$ and the resulting projected bubble fraction $\phi_0(t)$ defined by eq. (4) is shown
266 for the whole period studied in Fischer et al. (2017). We refer to this method as the *integral method*.

267
268 *Figure 4*

269
270 The method presented above is applicable only in boreholes and narrow tube-like mofettes. The borehole should tap
271 the underground water, and there should exist a continuous column of gas bubble flow from certain depth to surface.
272 Also, independent measurement of the hydraulic head in the aquifer/reservoir beneath the bubble flow column should
273 be possible, either in the same well or, at least, in a nearby well free of gas flow. These conditions are not fulfilled in
274 natural mofettes, which are usually only less than 2 m deep and communicate with the surface water significantly. In
275 such cases, the difference of pressure heads along a fixed depth interval *within* the bubble flow column can be
276 measured and used to define the mean bubble fraction $\overline{\phi}_{12}(t)$ and the projected bubble fraction $\phi_0(t)$.

277 This *differential method* has been tested in the Hartoušov well and Bublák mofette stations since 2015 using two
278 analog water-level sensors attached at a 1-meter distance on a metal rod. The obvious disadvantage is that both
279 measurements (instead of just one) are subject to fluctuation due to the bubbly flow, and that the noise in the resulting
280 bubble fraction data is inversely proportional to the distance between the probes. To suppress the noise, an RC circuit
281 with a 100 s time constant is applied.

282 An alternative way of determining the bubble fraction is based on the electric resistivity measurement of the water-
283 bubble mixture. Unlike the pressure difference method, this method does not need to be focused on the vertical chain
284 of bubbles, but it can assess the fraction of bubbles in a 3D volume defined by the geometry of electrodes. For this
285 purpose, two water resistivities are measured by a special probe in the mofette: the reference resistivity of the water
286 free of bubbles R_R and the resistivity of the water-bubble mixture R_M . The bubble fraction is then derived as
287

$$288 \quad \phi(t) = 1 - c \frac{R_R(t)}{R_M(t)}$$

289
290 where c is the geometric calibration constant. This type of measurement has been tested in the Soos mofette since
291 2015.

292

293 **2.4 Depth of gas bubbles appearance**

294 It is possible to speculate that the exsolution of the gas bubbles from the water with dissolved CO₂ takes place at a
295 certain depth in the borehole, while below that depth the pressure is sufficient to contain the CO₂ in the dissolved
296 phase. In this view, the exsolution depth d_e could vary in time, as considered by Fischer et al. (2017), following



297 variations of $h_e(t)$ and of the CO₂ supply from the reservoir. Let us note, however, that such a scenario is only possible
298 for gas fluxes much lower than those observed in the Hartoušov borehole.
299 Assuming a steady gas flow up through a borehole section with no penetration below d_e , two transport mechanisms
300 can be considered, convection or molecular diffusion. As for convection, no driving force to induce a flow in a water
301 column in a borehole, in particular no significant temperature variations, has been observed in the Hartoušov borehole.
302 The mass flux due to molecular diffusion, on the other hand, can be estimated as follows, and it appears to be very
303 limited. Assuming that the concentration of the dissolved CO₂ in the resting water column increases with increasing
304 depth as much as allowed by the increasing hydrostatic pressure (with the Henry's law constant being of the order of
305 $10^{-5} \text{ kg m}^{-3} \text{ Pa}^{-1}$, see Sander, 2015), then the corresponding diffusive flux (with the diffusivity being of the order of 10^{-9}
306 $\text{m}^2 \text{ s}^{-1}$) through the borehole of the given cross-section area (say, 10^{-2} m^2) would be no more than of the order 10^{-12} kg
307 s^{-1} . We thus infer that the gas bubbles enter the Hartoušov borehole in its penetrated section, as we assumed in the
308 previous section.

309

310 **2.5 Laboratory test of bubble fraction method**

311 The methodology for indirect gas flow measurement using pressure difference was first tested in the laboratory. The
312 experimental setup consisted of an air pump connected with a valve for controlling the air flow, which was led to the
313 bottom of a plastic tube with an inner diameter of 10.5 cm and a height of 2.5 m simulating the borehole. Two water
314 pressure probes were installed at a fixed distance of 0.5 m on a vertical rod inside the tube and all the air from this
315 tube was led to the chamber gas flowmeter. The air inflow was increased stepwise, and at each level the data were
316 recorded for a period of 15 min using a 1 Hz sampling rate. The gas flow ranged from 0 to 30 L/min, which corresponds
317 to the volumetric flux ranging from 0 to 0.06 m/s. The observed mean bubble fraction appears to increase nonlinearly
318 with the gas flow. Note that the modification using (Eq. 4) is insignificant here, due to the fact that both pressure
319 probes are at a depth of less than 1 m. The bubble fraction values are more scattered than the gas flow rate measured
320 by the flowmeter. The resulting noise was partially suppressed by low pass filtering of the pressure data using an RC
321 circuit with a time constant of 30 s and additionally by 1 min data sampling to smooth the water level values.

322 It is worth noting that the dynamics of bubbly flow in a borehole is quite a complex issue, which however appears to
323 have been studied rather intensively in the chemical and nuclear engineering literature (see, e.g., Ghiaasiaan, S.M.,
324 2008; Montoya, G. et al., 2016). The simple considerations introduced in the previous text (Eq. 3 and 4) correspond
325 to the drift-flux model for a vertical borehole, provided that the water flux through the borehole is negligible. In
326 particular, any momentum exchange with the walls is ignored. While this approach is well justified for the bubbly
327 flow regime observed with small gas fluxes, with increasing volumetric gas one observes different flow regimes of
328 greater complexity, such as the slug flow and churn flow. As the bubbles ascend, they increase in volume, join each
329 other merrily or even sadly split apart, their brief life being eventually cut short by obstacles such as the pressure
330 probes dangling in the well; these are however out of the scope of this paper. Even in the bubbly flow regime, the
331 relation between the bubble fraction ϕ and the volumetric flux of the gas bubbles u [m/s] has been described, e.g., by
332 the following well established empirical relation (Zuber, Findley, 1965).



333
$$\phi = \frac{u}{C_0 u + V_{gj}} \quad (5)$$

334 where $C_0 = 1.13$ and, assuming that the density of the gas is negligible when compared to that of water,

335
$$V_{gj} = 1.41 \left(\frac{\sigma g}{\rho_w} \right)^{1/4}$$

336 The curve in Fig. 5 is obtained by taking the surface tension for water and air at the laboratory temperature as
337 $\sigma = 0.07$ N/m. It appears that the mean bubble fractions derived from our pressure probe data overestimate the void
338 fractions given by the Zuber-Findley model, in particular for low flow rates. For comparison, we append to Fig. 6 the
339 projected bubble fraction data ϕ_0 plotted against the corresponding gas flow rates measured in the Hartoušov site. The
340 comparison to the laboratory data and to the Zuber-Findley model reveals a discrepancy that indicates some need for
341 further analysis, which is beyond the scope of the present study. Let us briefly note that the difference cannot be
342 explained by the mere parametric differences from the laboratory setting such as the temperature, gas and water
343 composition.

344 While it appears that the projected bubble fraction data from the Hartoušov site cannot be directly inverted to obtain
345 a reasonable gas flow rate estimate, it is important that they provide a fair correlation (see also Fischer et al. 2017 and
346 Fig. 4 in their paper) and can thus provide a valuable gas flow rate proxy. As expected, the integral method data seems
347 to perform better than the less recent differential data (see Section 2.3). Note particularly the high noise of the latter
348 and its lower correlation to the gas flow rate measurement (Fig. 6). Accordingly, using the pressure sensors at a larger
349 distance, and, if possible, placing one of them below the bubble entry depth, seem preferable for indirect gas flow
350 measurement.

351 *Figure 5*

352 *Figure 6*

353

354 2.6 Environmental effects

355 The measurements of CO₂ flow, CO₂ pressure and pressure head are influenced by environmental effects – mainly
356 variations of temperature (diurnal, seasonal), changes of barometric pressure and tidal effects. Temperature and
357 barometric changes are the most significant, since their influence can be local and can vary even among the stations
358 of the network. Barometric and tidal loading of aquifers has been studied in detail (e.g. Jacob, 1939; Rojstaczer and
359 Riley, 1990; Roeloffs, 1996). Here, we address the basic principles that are relevant to the pressure and production of
360 the upstreaming gas. Both the confined and unconfined response of pressure head are characterized by the barometric
361 efficiency E_B , which expresses the ratio of the change of the hydraulic head Δh caused by the barometric pressure
362 change Δb

363
$$E_B = \rho_w g \frac{\Delta h}{\Delta b} \quad (6)$$

364 The net response is always a decrease in the hydraulic head with an increase in barometric pressure. The barometric
365 pressure variations act directly on the open water level in the well and also on the formation composed of the mineral
366 matrix and pore space filled by the water. As a result, the direct effect on the water level in the borehole is partially



367 suppressed by the fraction of the external load borne by the formation water. Hence, the barometric efficiency can
368 also be written as

$$369 \quad E_B = \frac{\theta\beta}{\theta\beta + \alpha} \quad (7)$$

370 where α and β is the compressibility of the rock matrix and water, respectively, and θ represents porosity within the
371 aquifer. Thus, barometric efficiency can be described as the fraction of specific storage derived from the
372 compressibility of water or, equally, as the fraction of external load change borne by the formation either as
373 compaction or expansion. Accounting for the range of fractured rock compressibilities, E_B of confined aquifers usually
374 ranges between 0.2 and 0.7 (Todd, 1980) and may reach 1.0 for granite with a very low compressibility of the rock
375 matrix (Roeloffs, 1996; Acworth and Brain, 2008). Note, however, that large values of E_B may as well correspond to
376 large values of β ; this fact is not addressed in the literature for the simple reason that it is usually the rock that varies
377 from site to site and not the water. In this concern, the possible effect of the presence of the compressible CO₂ bubbles
378 within the aquifer surrounding the borehole on the barometric efficiency is a question that has not been addressed in
379 the literature, to the best of our knowledge.

380 Similarly, the barometric effect to the CO₂ discharge from an aquifer through an open well has not been studied either.
381 One can expect that an increase in the pore pressure due to an increase in the barometric pressure allows for larger
382 amounts of CO₂ to be dissolved in water, which in turn decreases the volume of CO₂ leaking into the well. Similarly,
383 a decrease in barometric pressure may induce increased degassing. Note that there exist many unknowns in this regard,
384 such as the flow paths of the gas ascending through the aquifer, the amount of the mobile and immobile gas bubbles
385 in the porous space, etc. In the Hartoušov borehole, a strong anticorrelation between the gas flow rate and the
386 barometric pressure has been observed.

387 Other external effects like diurnal temperature variations and Earth tides were found much weaker than the influence
388 of barometric pressure. The volumetric fraction of bubbles is not affected by air temperature, since the sensors are
389 placed in groundwater with an almost constant temperature. In addition, the periods of diurnal temperature variations
390 and significant Earth tide components are significantly shorter than the expected durations of anomalies of deep-
391 generated gas flow. Accordingly, we do not apply corrections for temperature variations and Earth tides.

392 We correct the measured quantity f (pressure head or gas flow) for demeaned barometric pressure variations b using
393 the equation $f_c = f - E_B (b - \langle b \rangle)$. Barometric efficiency E_B is determined with the target of minimum cross correlation
394 of f and f_c . To account for the possible time variation of E_B a sliding window of one day is used; see Fig. 7a for original
395 and corrected records of pressure head and gas flow in Hartoušov. Fig. 7b shows the cross-correlation functions
396 between barometric pressure and original and corrected records. The success of barometric correction is indicated
397 both by removing the anti-correlation with air pressure and by minimizing short period variations in the corrected
398 records. The mean barometric efficiency was 0.76 for the pressure head and 0.46 L/min/kPa for the gas flow.

399 *Figure 7*

400



401 3. Results of CO₂ flow monitoring in West Bohemia

402

403 The time series of gas production at all monitored stations, along with seismicity plot, are shown in Fig. 8. The record
404 at Hartoušov for the period from late 2007 to 2019 shows a long-term decrease interrupted by several abrupt massive
405 increases in gas production. The maximum flow, reaching 50 L/min, followed the 2014 seismic sequence in late
406 summer/autumn 2014; the minimum values, below 10 L/min, were observed prior to the 2014 seismic sequence and
407 at the present time. The fast coseismic increase and long-term postseismic decrease are visible both in the gas flow
408 and *integral bubble fraction* data determined using eq. (3) and (4) and are consistent with Sibson's fault valve model
409 (Fischer et al., 2017). Note particularly the abrupt rise in gas flow and CO₂ bubble fraction during the M_L 4.4 seismic
410 sequence of May – August 2014 and in bubble fraction during the October 2008 M_L 3.8 swarm. Next to these striking
411 coincidences of seismic activity and CO₂ release we also find cases of strong seismic activity, which was not
412 accompanied by a significant gas flow anomaly (see the M_L 3.4 swarm of 2011 and the most recent M_L 3.8 swarm of
413 2018). On the other hand, the CO₂ flow record shows a few positive pulses which are not related to significant seismic
414 activity (Fig. 8b). The most striking one is the gas production increase in the period from the beginning of May till the
415 end of July 2016, which is visible both in the gas flow and bubble fraction records. This is, however, undoubtedly of
416 anthropogenic origin caused by drilling of the nearby 108 m deep HJB-1 borehole at a distance of 40 m from the
417 monitored VP 8303 borehole, which drilling started on March 30 (Bussert et al., 2017). The drilling reached the ceiling
418 of a CO₂ pressured horizon at a depth of 80 m on April 21 and created a shortcut to the shallower aquifer, which was
419 tapped by the monitored borehole. The three-month long gas increase thus represents a delayed response to a nearby
420 drill. Another, less pronounced, positive pulse in the period from mid-September to late November 2016 is of unknown
421 origin. A number of negative pulses and oscillations are found on the bubble fraction record alone, which lower the
422 correspondence between the gas flow rate and the bubble fraction data and indicate a more complex relation between
423 gas flow in a borehole and volume fraction of ascending bubbles, as already noted in section 2.5.

424 The records of gas *differential bubble fraction* data in Bublák and *resistivity-based bubble fraction* in Soos indicate in
425 the monitored period since autumn 2015 a steady gas release with only a few bumps, which are most probably of local
426 origin and related to the shallow character of the mofettes. Gas at these sites passes through approximately cylindrical
427 vents of ~0.5 m diameter and ~1 m depth filled by surface water. The similarity of bubble fraction increase at Soos
428 and gas flow increase at Hartoušov in summer 2016 is most probably merely accidental, considering the anthropogenic
429 origin of the rise at Hartoušov and the large mutual distance of about 5 km of these sites.

430 As mentioned in section 2.3, the integral method of bubble fraction measurement provides better results than the
431 differential method. The latter suffers particularly from high noise caused by the placement of both pressure probes in
432 a water column with flowing bubbles as shown in Fig. 5. One can also notice a better correlation of the integral method
433 compared to the differential one. Unfortunately, due to technical problems, we were not able to perform this
434 comparison for the same time window – so time windows of the same length (3 months) free of any technical issues
435 were selected.

436



437 4. Discussion

438 The *barometric efficiency* E_B of the groundwater pressure head of 0.76, which we obtained, is relatively high. The
439 high values of E_B are generally considered an indication of the small compressibility of the rock matrix that is typical
440 for unweathered granite (Acworth and Brain, 2008). The target aquifer is formed by sedimentary formations of the
441 Cheb Basin composed of sandstones and conglomerates with varying clay contents underlain by mica-schist
442 basement (Bussert et al., 2017). The compressibility of these types of rocks is, however, 3 to 6 times greater than of
443 granite (their bulk moduli range from 10 to 20 GPa compared to 50 GPa for granite). Using Eq. (4), porosity 30% and
444 bulk moduli ratio of matrix and pore fluid equal to 5, one gets $E_B = 0.5$. The level $E_B = 0.76$ is reached for bulk moduli
445 ratio of 15. Assuming the bulk modulus of aquifer rocks about 10 GPa, one obtains a bulk modulus of the fluid of only
446 about 0.7 GPa, which corresponds to three times larger compressibility than for water. This could be explained by the
447 presence of carbon dioxide in the groundwaters in gaseous phase and is worth further research.

448 *The gas flow trend* in Hartoušov after the 2014 seismic sequence shows signatures similar to those in the period before
449 2014, which followed the 2008 swarm. A similar, long-term overall decrease is followed by steady state behavior with
450 an almost constant flow rate of about 10 L/min. In terms of the Sibson's fault valve model, this corresponds to the
451 self-sealing phase of the fault due to mineral precipitation (Sibson, 1992) when pressure builds up and in combined
452 action with tectonic loading results in increasing instability of the fault. This inevitably leads to later recurrence of
453 fault failure in the form of seismic activity and regeneration of fault permeability. As indicated above, the coincidence
454 of a massive rise in CO₂ flow and seismic activity has not been observed since the 2014 seismic sequence. Indeed,
455 none of the earthquake swarms since 2014 have been accompanied by a distinct CO₂ degassing anomaly (Fig 8b). All
456 in all, in the whole period of CO₂ flow monitoring in Hartoušov since 2007, five earthquake swarms with magnitude
457 M_L larger than 3.0 occurred (2008, 2011, 2014, 2017, 2018) and only two of them (2008 and 2014) were accompanied
458 by a strong and long-lasting coseismic increase in CO₂ degassing. This is not surprising in general, because the fault
459 valve mechanism might act only under certain circumstances. And even if a fluid pulse is released during every
460 stronger seismic sequence its volume might not be sufficient to reach the Earth's surface with a detectable amplitude.
461 This is also directly related to the pressure buildup in the fluid reservoir beneath the sealed fault, which is a long-
462 lasting process and thus earthquakes that occur soon after releasing the accumulated fluid pressure are likely to not be
463 accompanied by a significant fluid release. Recently, since the summer of 2019, the CO₂ flow rate in Hartoušov has
464 decreased below 10 L/min, which could be a sign of the approaching occurrence of a new seismic swarm, according
465 to the Sibson's fault valve model.

466 In this context it is also of interest to consider the *hypocenter cluster geometry* in 3D and its relation to the presence
467 of permeable channels in a shallow crust allowing crustal fluids to reach the surface. In Fig. 9 hypocenters of individual
468 earthquake sequences are indicated in a vertically oriented cross section and show a hat-like structure in depths from
469 6.0 to 10.5 km extending about 10 km north-south. The Hartoušov mofette field is located about 10 km south from
470 the center of the main cluster, which corresponds to 6 km distance from its southern tip. A pronounced segmentation
471 of the fault plane is apparent with the 2008 and 2014 segments in the southern branch of the cluster and the 2011,
472 2017 and 2018 segments clusters in its northern branch. It is worth noting that the 2014 mainshocks showed
473 unfavorable oriented focal mechanisms and occurred on a fault jog activated by stress concentration resulting from



474 previous swarm activity (Hainzl et al., 2016, Jakoubková et al. 2018). This structural and possibly impermeable
475 boundary within the fault zone was broken by the M_L 3.5 mainshock of the 2014 sequence - the first earthquake of
476 this sequence which was followed by the massive CO₂ flow rise in Hartoušov.

477 The clear coseismic CO₂ flow rate increase during the 2008 and 2014 seismic sequences indicates the presence of a
478 *permeable channel between the southern cluster and the Hartoušov mofette field* (Fig. 9). The absence of CO₂ flow
479 anomalies coinciding with the seismic activity in northern clusters could be interpreted to show that the hydraulic
480 connection between these fault patches and the Hartoušov mofette is missing, which could be related to the afore-
481 mentioned fault jog. Besides, it is also of interest that epicenter distribution and CO₂ degassing occurrence is typically
482 separated in the area (Weinlich et al., 2006; Babuška and Plomerová, 2008); most earthquakes occur in the northern,
483 CO₂-free part of the Cheb Basin.

484 *Other monitored sites* such as Bublák and Soos show, similar to Hartoušov, almost constant CO₂ discharge since early
485 2017. As these stations were not in operation during the 2008 and 2014 seismic sequences showing coseismic CO₂
486 increase in Hartoušov, no inferences about their correlation to the seismic activity can be drawn. Continuous
487 monitoring of CO₂ degassing is required to determine whether future seismic activity in the southern cluster will
488 generate an increase in degassing in either of the monitored sites and enable the verification of the hypothesis that
489 only earthquakes in the southern cluster are capable of generating a CO₂ pulse which reaches the surface.

490 5. Conclusions

491 The present study is focused on the long-term monitoring of CO₂ degassing in the form of mofettes and gaseous
492 mineral springs targeted on the West Bohemia/Vogtland region in Central Europe, which is typified by the occurrence
493 of earthquake swarms and emanations of carbon dioxide of magmatic origin. The gas flow measurement is applied to
494 two types of sources: natural wet mofettes with gas outflow through surface water pools and boreholes tapping shallow
495 CO₂-saturated aquifers. The different local conditions of the five monitored sites call for different methods of gas
496 capture and flow rate measurement. Besides the direct flow measurement using a drum chamber gas flowmeter,
497 electronic MEMS flowmeters and Venturi-based probes we introduce a novel, indirect method based on quantifying
498 the gas bubble contents in a water column, which is capable of functioning in severe environmental conditions. The
499 method is based on measuring the pressure difference along a fixed depth interval in a water column, which is
500 proportional to the mean bubble fraction within the measured section. We analyze the dependence of the bubble
501 fraction on depth and project it to the atmospheric pressure to make it directly comparable to the gas flow rate.
502 Laboratory tests indicate the nonlinear dependence of the bubble fraction on the flow rate, which is confirmed by
503 empirical models found in the chemical and nuclear engineering literature. Flow rates and bubble fractions observed
504 in a pilot borehole in the Hartoušov mofette show a high mutual correlation, however some discrepancy is found
505 between the measured flow rate and that predicted by the empirical models. This discrepancy calls for further
506 analysis.

507 We also analyzed the long-term monitoring of gas flow and bubble fraction in the pilot borehole for the period 2008
508 – 2019. We found a quite strong barometric influence on the hydraulic head of the confined aquifer corresponding to



509 a barometric efficiency of 0.76, which can be attributed to the compressibility of the pore fluids including the gaseous
510 phase of carbon dioxide.

511 The record of gas flow rate and bubble fraction in Hartoušov shows two high-amplitude coseismic rises coinciding
512 with the occurrence of earthquake swarms in 2008 and 2014. The flow rate increased to a multitude of the preseismic
513 level for several months and was followed by a long-term decay. However, another three seismic swarms occurring
514 in the same fault zone were not associated with any significant CO₂ flow anomaly. We surmise that this may be related
515 to the slightly farther location of hypocenters of these swarms in comparison with the two which caused the coseismic
516 CO₂ flow rise. Further long-term CO₂-flow monitoring is required to verify the mutual influence of CO₂ degassing
517 and seismic activity in the area.

518 **Code/Data availability**

519 Most of the data analyzed in the manuscript including email address for requesting additional data are available
520 online at web.natur.cuni.cz/uhigug/carbonnet/en_index.html.

521

522 **Author's contribution**

523 VB and TF designed and carried out the measurements and ML formulated the theoretical part with support of TF. TF
524 prepared the manuscript with contributions from all co-authors.

525

526 **Competing interests**

527 The authors declare that they have no conflict of interest.

528

529 **Acknowledgments**

530 CO₂ flow monitoring and the work of the authors was supported by the project CzechGeo/EPOS-Sci
531 (CZ.02.1.01/0.0/0.0/16_013/0001800). The authors thank also to Jan Vilhelm for valuable ideas.

532



533 **References**

534

535 Acworth R.I. and Brain T., Calculation of barometric efficiency in shallow piezometers using water levels,
536 atmospheric and earth tide data. *Hydrogeology Journal* 16, 1469–1481, 2008.

537 Babuška V., Plomerová J., Control of paths of quaternary volcanic products in Western Bohemian Massif by
538 rejuvenated variscan triple junction of ancient microplates. *Stud. Geophys. Geod.*, 52, 607-629, 2008.

539 Babuška, V., et al., Origin of earthquake swarms in the western Bohemian Massif: Is the mantle CO₂ degassing,
540 followed by the Cheb Basin subsidence, an essential driving force?, *Tectonophysics* 668-669, 42-51,
541 <http://dx.doi.org/10.1016/j.tecto.2015.12.008>, 2016.

542 Bachura, M. and Fischer T., Detailed velocity ratio mapping during the aftershock sequence as a tool to monitor the
543 fluid activity within the fault plane. *Earth and Planetary Science Letters* 453, 215–222.
544 <https://doi.org/10.1016/j.epsl.2016.08.017>, 2016.

545 Bankwitz, P., Schneider, G., Kämpf, H., Bankwitz, E., Structural characteristics of epicentral areas in Central Europe:
546 study case Cheb Basin (Czech Republic). *J. Geodyn.* 35, 5–32, 2003.

547 Baubron, J. C., Allard P., Toutain J. P., Diffuse volcanic emissions of carbon dioxide from Vulcano island, Italy,
548 *Nature*, 344, 51–53, 1990.

549 Bräuer, K., Kämpf, H., Strauch, G., Weise, S.M., Isotopic evidence (³He/⁴He, ¹³C CO₂) of fluid-triggered intraplate
550 seismicity. *J. Geophys. Res.* 108 (B2), 2070. <http://dx.doi.org/10.1029/2002JB002077>, 2003.

551 Bräuer, K., Kämpf, H., Niedermann, S., Strauch, G., Tesař, J., Natural laboratory NW Bohemia: comprehensive fluid
552 studies between 1992 and 2005 used to trace geodynamic processes. *Geochem. Geophys. Geosyst.* 9,
553 <http://dx.doi.org/10.1029/2007GC001921> (Q04018), 2008.

554 Bussert R., Kämpf H., Flechsic C., Hesse K., Nickschick T., Liu Q., Umlauft J., Vylita T., Wagner D., Wonik T.,
555 Flores H.E., and Alawi M., Drilling into an active mofette: pilot-hole study of the impact of CO₂-rich mantle-derived
556 fluids on the geo–bio interaction in the western Eger Rift (Czech Republic). *Sci. Dril.*, 23, 13–27,
557 <https://doi.org/10.5194/sd-23-13-2017>, 2017.

558 Camarda, M., S. Gurrieri, and M. Valenza., CO₂ flux measurements in volcanic areas using the dynamic concentration
559 method: Influence of soil permeability, *J. Geophys. Res.*, 111, B05202, doi:10.1029/2005JB003898, 2006.

560 Dahm, T., Fischer, T., Velocity ratio variations in the source region of earthquake swarms obtained from arrival time
561 double-differences. *Geophys. J. Int.* 196, pp. 957-970. URL: <http://dx.doi.org/10.1093/gji/ggt410>, 2014.

562 Dmytriw, A. M., Kilian, W. T., Speldrich, J. W., Beck, S. E., Morales, G., and Gehman, R. W., U.S. Patent No.
563 7,278,309. Washington, DC: U.S. Patent and Trademark Office, 2007.

564 Ellingsen, K., and Risso, F., On the rise of an ellipsoidal bubble in water: oscillatory paths and liquid-induced velocity.
565 *Journal of Fluid Mechanics*, 440, 235-268, 2001.



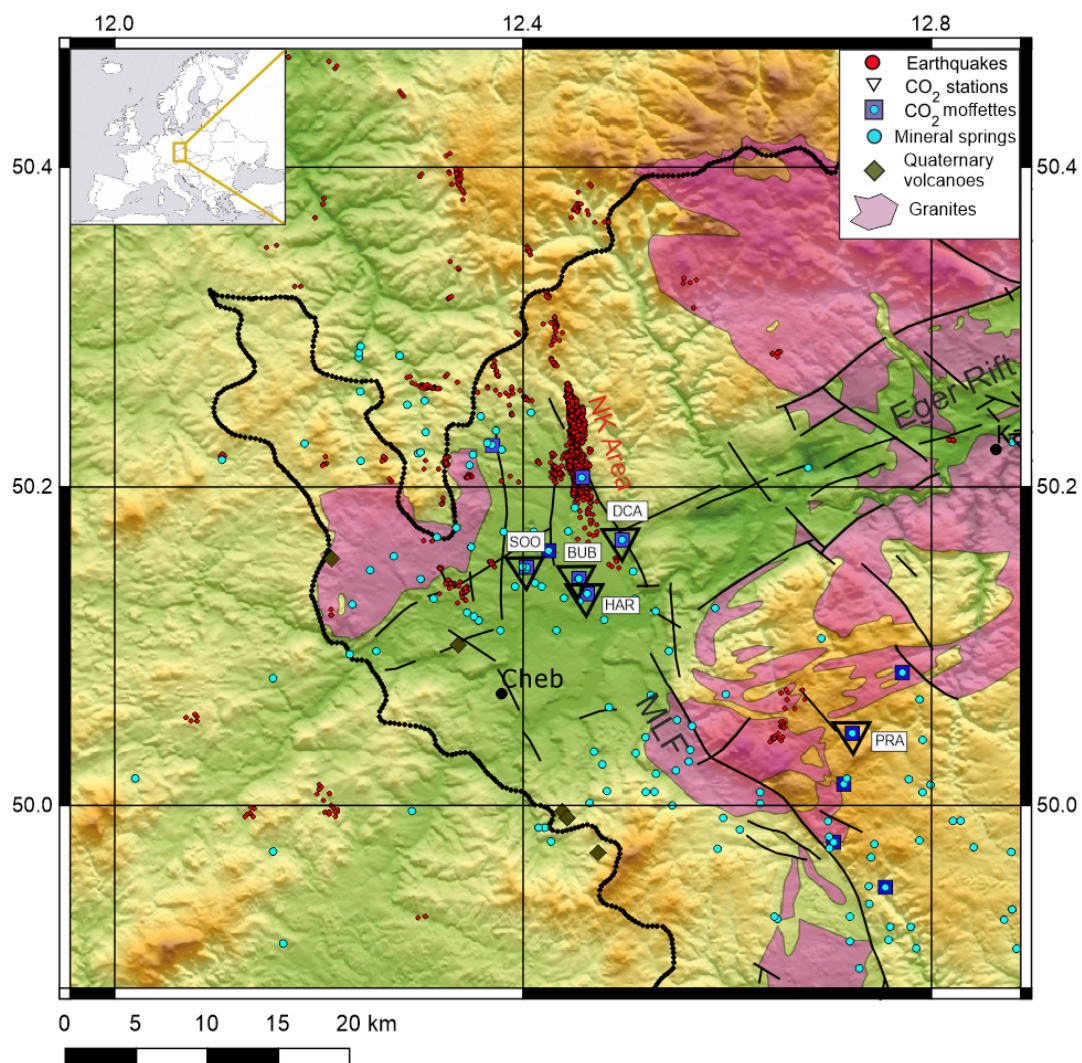
- 566 Faber, E., Horálek, J., Boušková, A., Teschner, M., Koch, U., and Poggenburg, J., Continuous gas monitoring in the
567 West Bohemian earthquake area, Czech Republic: First results. *Studia Geophysica et Geodaetica*, 53(3), 315-328,
568 2009.
- 569 Fischer, T., Horálek, J., Slip-generated patterns of swarm microearthquakes from West Bohemia/Vogtland (central
570 Europe): evidence of their triggering mechanism. *J. Geophys. Res.* 110, B05S21.
571 <http://dx.doi.org/10.1029/2004JB003363>, 2005.
- 572 Fischer, T., Horálek, J., Hrubcová, P., Vavryčuk, V., Bräuer, K., Kämpf, H., Intra-continental earthquake swarms in
573 West-Bohemia and Vogtland: a review, *Tectonophysics* 611, 1-27, doi: 10.1016/j.tecto.2013.11.001, 2014.
- 574 Fischer, T., Matyska, C., and Heinicke., Earthquake-enhanced permeability—evidence from carbon dioxide release
575 following the ML 3.5 earthquake in West Bohemia. *Earth and Planetary Science Letters*, 460, 60-67, 2017.
- 576 Franke, W., The mid-European segment of the Variscides: tectonostratigraphic units, terrane boundaries and plate
577 tectonic evolution. In: Franke, W., Haak, V., Oncken, O., Tanner, D. (Eds.), *Orogenic Processes: Quantification and*
578 *Modelling in the Variscan Belt*, vol. 179. *Geol. Soc., Spec. Publ.*, London, pp. 35–61, 2000.
- 579 Geissler, W.H., Kämpf, H., Kind, R., Klinge, K., Plenefisch, T., Horálek, J., Zedník, J., Nehybka, V., Seismic structure
580 and location of a CO₂ source in the upper mantle of the western Eger rift, Central Europe. *Tectonics* 24 (TC5001).
581 <http://dx.doi.org/10.10292004TC001672>), 2005.
- 582 Ghiaasiaan, M.S., *Two-phase flow, boiling and condensation in conventional and miniature systems*. Cambridge
583 University Press. 636p, 2008.
- 584 Gurrieri, S., Valenza M., Gas transport in natural porous medium: a method for measuring soil CO₂ flows from the
585 ground in volcanic and geothermal areas, *Rend. Soc. Ital. Mineral. Petrol.*, 43, 1151–1158, 1988.
- 586 Hainzl, S., Fischer, T., Indications for a successively triggered rupture growth under – lying the 2000 earthquake
587 swarm in Vogtland/NW-Bohemia. *J. Geophys. Res.* 107 (B12), 2338. <http://dx.doi.org/10.1029/2002JB001865>.
588 2002.
- 589 Hainzl, S., Fischer, T., Čermáková, H., Bachura, M., Vlček, J., Aftershocks triggered by fluid-intrusion: evidence for
590 the aftershock sequence occurred 2014 in West Bohemia/Vogtland. *J. Geophys. Res.*, *Solid Earth* 121.
591 <http://dx.doi.org/10.1002/2015JB012582>, 2016
- 592 Heinicke, J., Koch, U., Slug flow — a possible explanation for hydrogeochemical earthquake precursors at Bad
593 Brambach, Germany. *Pure Appl. Geophys.* 157 (10), 1621–1641, 2000.
- 594 Horálek, J., Šílený, J., Fischer, T., Moment tensors of the January 1997 earthquake swarm in NW Bohemia (Czech
595 Republic): double-couple vs. non-double-couple events. *Tectonophysics* 356, 65–85, 2002.
- 596 Hron J., and Škuthan B., Continuing research into the pressure field of carbon-dioxide in the West-Bohemian spa
597 region (in Czech). *Czech Ministry of Environment, Prague*, 112 p, 2006.



- 598 Hrubcová, P., Geissler, W.H., Bräuer, K., Vavryčuk, V., Tomek, Č., Kämpf, H., Active magmatic underplating in
599 western Eger Rift, Central Europe. *Tectonics* 36. <https://doi.org/10.1002/2017TC004710>, 2017.
- 600 Jacob C.E., Fluctuations in artesian pressure produced by passing railroad-trains as shown in a well on Long Island,
601 New York. *Eos Trans. AGU*, 20(4), 666–674, doi:10.1029/TR020i004p00666, 1939.
- 602 Jakoubková, H., Horálek, J., and Fischer, T., 2014 mainshock-aftershock activity versus earthquake swarms in West
603 Bohemia, Czech Republic. *Pure and Applied Geophysics*, 175(1), 109–131. [https://doi.org/10.1007/s00024-017-](https://doi.org/10.1007/s00024-017-1679-7)
604 [1679-7](https://doi.org/10.1007/s00024-017-1679-7), 2018.
- 605 Kämpf, H., Geissler, W.H., Bräuer, K., Combined gas-geochemical and receiver func- tion studies, of the
606 Vogtland/NW-Bohemia intraplate mantle degassing field Central Europe. In: Ritter, J.R.R., Christiansen, U.R. (Eds.),
607 *Mantle Plumes — A Multidisciplinary Approach*. Springer-Verlag, Berlin-Heidelberg-New York, pp. 127–158., 2007.
- 608 Koch, U., Heinicke, J., and Voßberg, M., Hydrogeological effects of the latest Vogtland-NW Bohemian swarmquake
609 period (August to December 2000). *Journal of Geodynamics*, 35(1), 107-123, 2003.
- 610 Montoya, G.; Lucas, D.; Baglietto, E.; Liao, Y., A review on mechanisms and models for the churn-turbulent flow
611 regime. *Chem. Eng. Sci.* 141, 86-103. DOI 10.1016/j.ces.2015.09.011, 2016.
- 612 Nickschick T., Kämpf H., Flechsig C., Mrlina J., Heinicke J., CO₂ degassing in the Hartoušov mofette area, western
613 Eger Rift, imaged by CO₂ mapping and geoelectrical and gravity surveys. *Int J Earth Sci.*, 2015.
- 614 Roeloffs, E., Poroelastic techniques in the study of earthquake-related hydrologic phenomena, *Advances in*
615 *Geophysics*, 37, 135-195, 1996.
- 616 Rojstaczer, S. and Riley F. S., Response of the water level in a well to Earth tides and atmospheric loading under
617 unconfined conditions. *Water Resources Research*, 26 (8), 1803-1817, 1990.
- 618 Sander, R., Compilation of Henry's law constants (version 4.0) for water as solvent. *Atmos. Chem. Phys.*, 15, 4399-
619 4981, DOI 10.5194/acp-15-4399-2015, 2015.
- 620 Sibson, R.H., Implications of fault-valve behavior for rupture nucleation and recurrence. *Tectonophysics* 211, 283–
621 293, 1992.
- 622 Škuthan B., Hron J., Pěček J. and Kepřta M., Carbon dioxide field in the West Bohemian Spring Region: Introductory
623 results. *Bull. Czech Geol. Surv.*, 76/4, 203–208, 2001.
- 624 Špičák, A., Horálek, J., Migration of events during the January 1997 earthquake swarm (The West Bohemia–Vogtland
625 region). *Stud. Geophys. Geod.* 44, 227–232, 2000.
- 626 Špičáková, L., Uličný, D., Koudelková, G., Tectonosedimentary evolution of the Cheb Basin (NW Bohemia, Czech
627 Republic) between Late Oligocene and Pliocene: a preliminary note. *Studia Geophys. Geod.* 44, 556–580, 2000.
- 628 Todd D.K., 1980. *Groundwater Hydrology*. 2d ed. New York: John Wiley & Sons.



- 629 Vavryčuk, V., Non-double-couple earthquakes of January 1997 in West Bohemia, Czech Republic: evidence of tensile
630 faulting. *Geophys. J. Int.* 149, 364–373. <http://dx.doi.org/10.1046/j.1365-246X.2002.01654.x>, 2002.
- 631 Vavryčuk, V., Principal earthquakes: theory and observations from the 2008 West Bohemia swarm. *Earth Planet. Sci.*
632 *Lett.* 305, 290–296. <http://dx.doi.org/10.1016/j.epsl.2011.03.002>, 2011.
- 633 Vavryčuk, V., and P. Hrubcová, Seismological evidence of fault weakening due to erosion by fluids from observations
634 of intraplate earthquake swarms, *J. Geophys. Res. Solid Earth*, 122, doi:10.1002/2017JB013958, 2017.
- 635 Weinlich, F.H., Bräuer, K., Kämpf, H., Strauch, G., Tesar, J., Weise, S.M., An active sub – continental mantle volatile
636 system in the western Eger rift, Central Europe: gas flux, isotopic (He, C, and N) and compositional fingerprints.
637 *Geochim. Cosmochim. Acta* 63, 3653–3671. [http://dx.doi.org/10.1016/S0016-7037\(99\)00187-8](http://dx.doi.org/10.1016/S0016-7037(99)00187-8), 1999.
- 638 Weinlich, F. H., Faber, E., Boušková, A., Horálek, J., Teschner, M., and Poggenburg, J., Seismically induced
639 variations in Mariánské Lázně fault gas composition in the NW Bohemian swarm quake region, Czech Republic—A
640 continuous gas monitoring. *Tectonophysics*, 421(1), 89-110, 2006.
- 641 Ziegler, P.A., European Cenozoic rift system. *Tectonophysics* 208, 91–111, 1992.
- 642 Zuber, N., and Findlay, J., Average volumetric concentration in two-phase flow systems. *Journal of heat transfer*,
643 87(4), 453-468, 1965
644
645
646



647

648

649

650

651

652

653

Figure 1. Relief map of the West Bohemia/Vogtland region with the fault network, granite units, and major fault zones as Mariánské Lázně Fault (MLF) and Eger Rift. Seismic events, major focal zone of Nový Kostel (NK Area), CO₂ monitoring stations, CO₂ mofettes and mineral springs and Quaternary volcanoes are also indicated (see the legend).



654

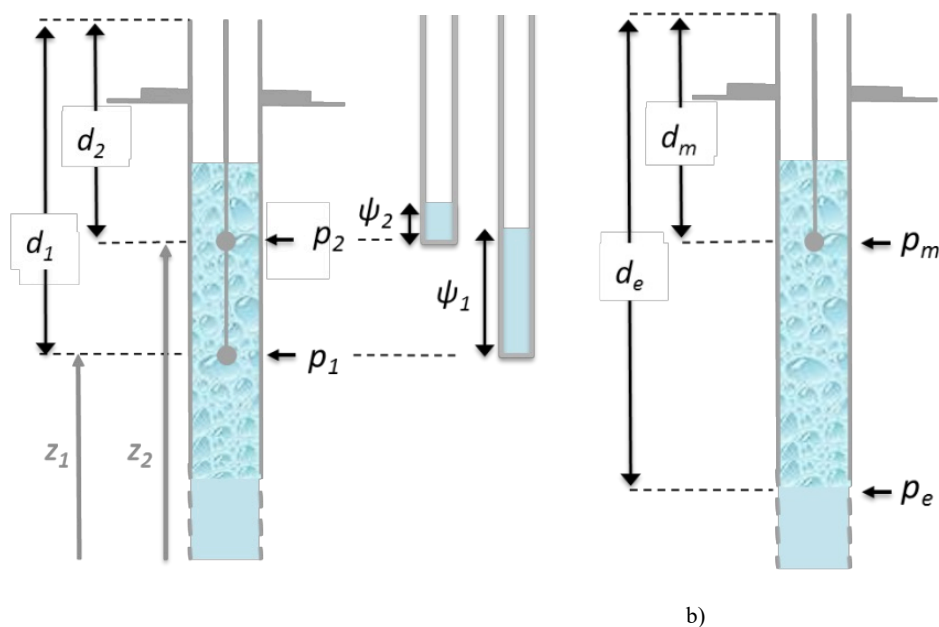
655 **Figure 2. Photos of selected CO₂ monitoring fields – Hartoušov, SOOS, Bublák and Prameny**

656

657



658



659

660 a)

b)

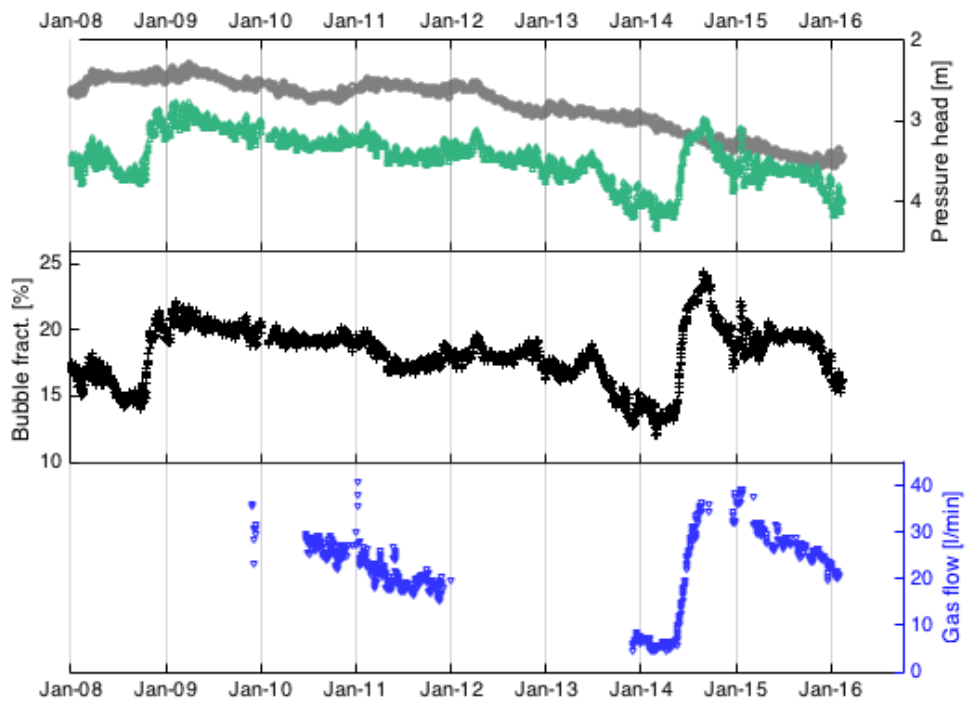
661 **Figure 3.** Measurement of pressure in the borehole with ascending bubbles: the measured pressure p and the related
662 pressure head ψ at two different depths d_1 and d_2 within the bubble column using the *differential method* (a); pressure
663 within the bubble column p_m and beneath p_e used to determine the mean bubble fraction using the *integral method* (b). Note
664 that the difference of altitudes $z_2 - z_1 = d_e - d_m$.

665

666

667

668

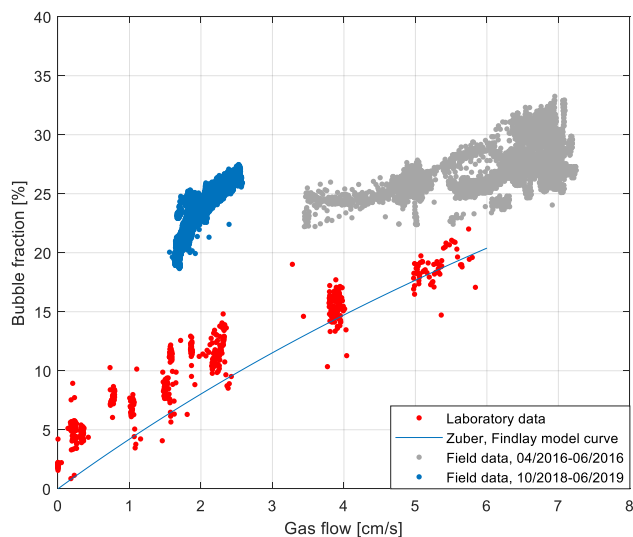


669

670 **Figure 4.** Daily averages of pressure head h_e in the reference well (grey) unaffected by gas flow and in the monitored
671 Hartoušov well, h_m (green); the volumetric fraction of bubbles (black) determined by Eq. 4 and CO₂ flow (blue) in the
672 Hartoušov well for the period 2008-2016.

673

674

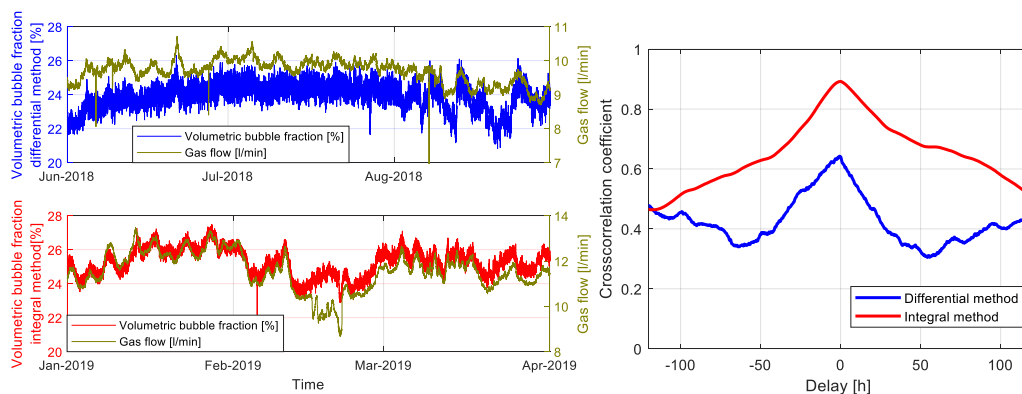


675

676 **Figure 5. Comparison of gas flow and volumetric fraction of bubbles for the field (Hartoušov mofette) and laboratory**
 677 **measurement. Laboratory measurements are smoothed by RC circuit of 30 s time constant (red points) and additionally by**
 678 **running average of 1 min length; the field measurements from 2016 (grey points) are based on the differential method with**
 679 **sensor distance of 1.0 m; the field measurements from 2018-2019 (blue points) are based on the integral method. Blue line**
 680 **is the best fit based on eq. (5).**

681

682



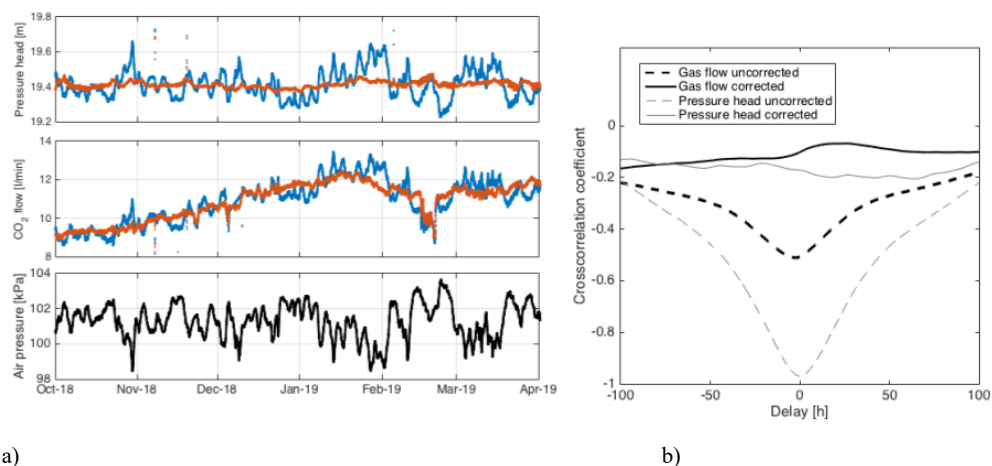
683

684 **Figure 6. Comparison of volumetric bubble fraction derived using integral and differential methods with the gas flow at**
 685 **the Hartoušov site. Depth of pressure probes for the differential method are 4.45 and 5.45 m below the surface. For the**
 686 **integral method it is 5.45 m and 27.2 m.**

687



688



689

690

691

692

693

694

695

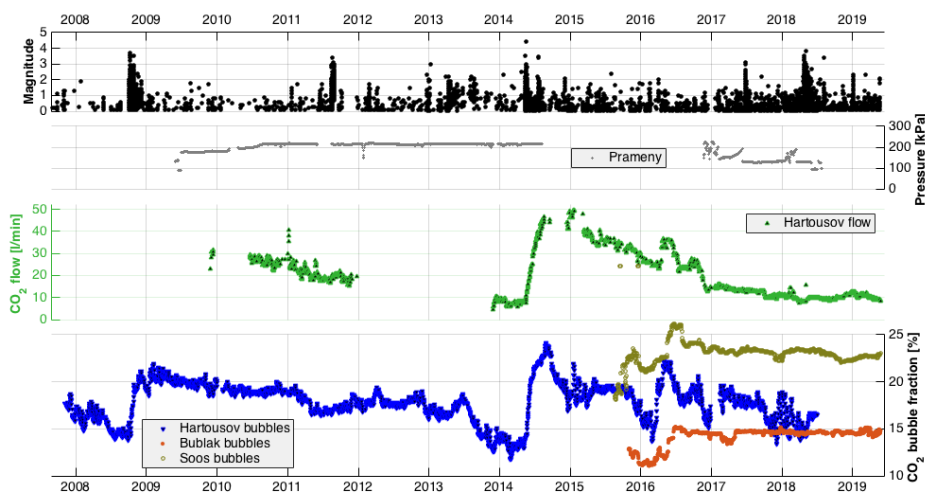
696

697

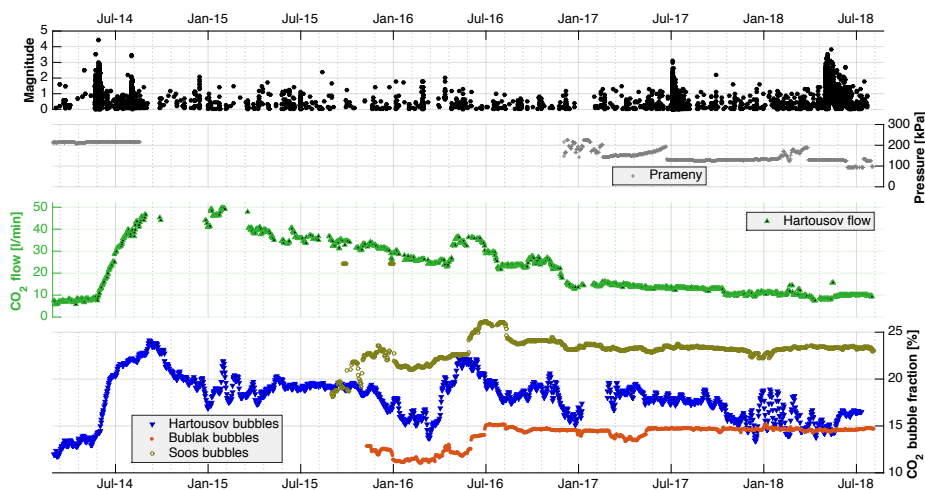
a)

b)

Figure 7. The barometric effect to the pressure head and CO₂ flow in the Hartoušov borehole for the period from October 2018 to April 2019. a) Original measurements are indicated in blue and those corrected for barometric pressure are in red. The upper panel shows pressure head at the depth below the bubble formation and the lower panel shows gas flow measured by flowmeter. The success of barometric correction is illustrated in b) showing the decrease of barometric anticorrelation after correcting.



698
699 a)

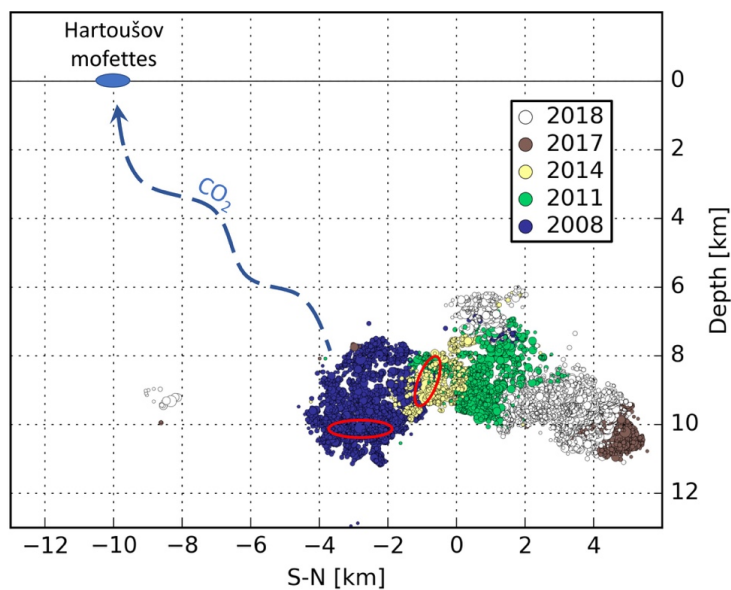


700
701 b)

702

703 **Figure 8.** Comparison of seismic activity and CO₂ production at individual monitoring sites in West Bohemia. For
704 Hartoušov the CO₂ flow and gas bubble fraction are shown; for Bublák and Soos the CO₂ bubble fraction is shown and for
705 Prameny the gas pressure in a closed borehole is plotted; (a) period 2007-2019; (b) detail for the period 2014-2019. Gas
706 bubble fraction was determined using the integral method.

707



708
709
710
711

Figure 9. Vertical, north-south oriented section through the Nový Kostel fault zone with hypocenters of the earthquake swarms occurred between 2008 and 2018. The position of the Hartoušov mofette showing coseismic CO₂ flow rate increase is indicated on the surface. Red ovals show the position of first events of the 2008 and 2014 seismic sequences.